BASIC SCIENCE

Nanomedicine: Nanotechnology, Biology, and Medicine
37 (2021) 102438

Original Article

nanomedjournal.com

RNA-dependent assembly of chimeric antigen nanoparticles as an efficient H5N1 pre-pandemic vaccine platform

Jongkwan Lim, MS[a], Yucheol Cheong, BS[a], Young-Seok Kim, PhD[a], Wonil Chae, PhD[a], Beom Jeung Hwang, PhD[a], Jinhee Lee, PhD[b], Yo Han Jang, PhD[c], Young Hoon Roh, PhD[a,*], Sang-Uk Seo, PhD[d,*], Baik L. Seong, PhD[a,e,f,**]

[a]*Department of Biotechnology, College of Life Sciences and Biotechnology, Yonsei University, Seoul, Republic of Korea*
[b]*Department of Integrated OMICS for Biomedical Science, College of Life Sciences and Biotechnology, Yonsei University, Seoul, Republic of Korea*
[c]*Department of Biological Sciences and Biotechnology, College of Life Sciences and Biotechnology, Andong National University, Andong, Republic of Korea*
[d]*Department of Microbiology, College of Medicine, The Catholic University of Korea, Seoul, Republic of Korea*
[e]*Department of Microbiology, College of Medicine, Yonsei University, Seoul, Republic of Korea*
[f]*Vaccine Innovative Technology Alliance-Korea, Yonsei University, Seoul, Republic of Korea*

Revised 12 May 2021

Abstract

Highly pathogenic avian influenza viruses (HPAIVs) pose a significant threat to human health, with high mortality rates, and require effective vaccines. We showed that, harnessed with novel RNA-mediated chaperone function, hemagglutinin (HA) of H5N1 HPAIV could be displayed as an immunologically relevant conformation on self-assembled chimeric nanoparticles (cNP). A tri-partite monomeric antigen was designed including: i) an RNA-interaction domain (RID) as a docking tag for RNA to enable chaperna function (chaperna: chaperone + RNA), ii) globular head domain (gd) of HA as a target antigen, and iii) ferritin as a scaffold for 24 mer-assembly. The immunization of mice with the nanoparticles (~46 nm) induced a 25–30 fold higher neutralizing capacity of the antibody and provided cross-protection from homologous and heterologous lethal challenges. This study suggests that cNP assembly is conducive to eliciting antibodies against the conserved region in HA, providing potent and broad protective efficacy.

Key words: Ferritin nanoparticle; Self-assembly; Chaperna; Influenza vaccine; Hemagglutinin

Approximately 40 infectious diseases have been discovered since the 1970s, and vaccine development is urgently recommended for curbing the potential outbreak of pandemics, as outlined in the World Health Organization (WHO) blueprint list of priority diseases.[1,2] In particular, for newly discovered viruses, conventional cell culture often fails to produce enough vaccine doses in a timely manner. Subunit vaccines, as an alternative to cell culture techniques, are an attractive option for the development of vaccines for reasons including safety and manufacturing scalability.[3] Recombinant nanoparticles (NPs) have been considered a high-priority vaccine strategy to enhance the antibody response to subunit vaccines. NP formation increases the density of antigens and allows their controlled distribution to elicit an efficient immune response.[4] NPs can be produced in recombinant hosts without biosafety concerns, providing an efficient and cost-effective means of vaccine production.[5,6] However, the multivalent display of vaccine antigens on the surface of NPs as a chimeric construct increases the kinetic complexity of the protein folding. In most cases, this results in the formation of inclusion bodies with immunologically irrelevant conformations. Hence, failure of regular assembly of monomers is common in vaccine design, as it relies on the refolding of inclusion bodies before regular assembly into multimeric complexes.[7,8] The structure-based vaccine design based on the thermodynamic stability of the antigen eventually

Conflict of interest: All authors declare that there are no conflicts of interest.

Support: This work was supported by the Korea Health Technology R&D Project through the Korea Health Industry Development Institute (KHIDI), the Ministry of Health & Welfare, Republic of Korea [grant number HV20C0070]; the National Research Foundation of Korea [grant number 2018M3A9H4079358]; Brain Korea 21 (BK21) FOUR program.

* Corresponding authors.
** Correspondence to: B.L. Seong, Department of Biotechnology, College of Life Sciences and Biotechnology, Yonsei University, Seoul, Republic of Korea.
E-mail addresses: yr36@yonsei.ac.kr, (Y.H. Roh), suseo@catholic.ac.kr, (S.-U. Seo), blseong@yonsei.ac.kr. (B.L. Seong).

https://doi.org/10.1016/j.nano.2021.102438

Please cite this article as: Lim J, et al, RNA-dependent assembly of chimeric antigen nanoparticles as an efficient H5N1 pre-pandemic vaccine platform. *Nanomedicine: NBM* 2021;37:102438, https://doi.org/10.1016/j.nano.2021.102438

increases the kinetic complexity in the folding pathway, which is vulnerable to misfolding or defective assembly into amorphous aggregates.[9–11] A technical breakthrough to enable the folding of chimeric antigens and their subsequent assembly still awaits NP-based recombinant vaccines.

One of the NP formation platforms, ferritin, self-assembles into 24-subunit particles with eight three fold axes at a distance (28 Å) nearly identical to the central axes of the trimer of viral surface proteins, such as influenza hemagglutinin (HA) or corona spike protein, making it an ideal platform for designing a recombinant vaccine antigen.[12,13] In addition, ferritin nanoparticle-based vaccines can induce the production of broadly neutralizing antibodies compared to antigen alone.[14–16] Moreover, two ferritin NP-based influenza HA vaccines have already been shown to be safe and immunogenic in clinical trials (NCT03186781, NCT03814720).[17,18] The display of antigens on the surface of ferritin NP requires chimeric constructs of various structural and functional domains, which in most cases requires a robust folding environment usually provided by eukaryotic hosts.[17,19,20]

Since 2003, the highly pathogenic avian influenza virus H5N1, one of the A/goose/Guangdong/1/96 lineage (GDL) viruses, has been associated with ~900 human infection cases and ~450 deaths (i.e., ~50% fatality rate).[21] Since egg-based vaccines require several months for production and are strictly dependent on the supply of eggs, the platform is inadequate for rapid and massive vaccine production during the pandemic outbreak.[22] The surface glycoprotein hemagglutinin (HA) is the most important antigen for influenza vaccine development. Recombinant HA protein vaccines are effective at inducing neutralizing antibodies and hence, are considered as an alternative to classical egg-grown inactivated vaccines against HPAI viruses.[23] The most widely used substrates for the expression of HA proteins are insect or mammalian cells,[24–26] which provide high-purity antigens with relatively low yields.[23,27] While bacterial cells provide an easy and economical system for the production of HA proteins,[28] viral proteins expressed in *Escherichia coli* cells are usually expressed as insoluble aggregates and require a refolding process in the presence of high concentrations of chaotropic agents such as urea or guanidine hydrochloride.[29–31]

Here, we present a novel platform for the assembly of influenza HA in the form of chimeric nanoparticles (cNPs) in *E. coli* without refolding, capitalizing on the function of an RNA-based chaperone. Distinct to protein-based molecular chaperones, RNAs provide extremely versatile chaperone functions (chaperna: chaperone + RNA), probably in operation as early as in the ancient "RNA World," for the folding and assembly of monomers into nanostructures.[32] In this study, the globular domain of H5N1 HA (H5gd), as an antigen, was fused with the RID and bacterioferritin (Bfr) to construct a nanoparticle vaccine presenting the trimeric HA protein. The self-assembled cNP purified from *E. coli* was confirmed by physicochemical tests such as size exclusion chromatography (SEC), transmission electron microscopy (TEM), and dynamic light scattering (DLS). In addition, the protective efficacy of the recombinant vaccine was validated by functional assays of neutralizing antibodies *in vitro*, mouse lethal challenge, and cross-clade reactivity. Taken together, our strategy provides a novel methodology for the fast and enhanced delivery of low-cost NP-based vaccines against viral infections.

Methods

3D structure modeling

3D structural modeling of RID-H5gd-Bfr was performed using MODELLER (Version 9.20, Andrej Sali, USA). To obtain the RID-H5gd-Bfr structure, the structure of H5gd was generated by I-TASSER web software. The fusion structures, including the N-terminally fused RID to H5gd based on the structure of human KRS (PDB ID: 1BBU) and C-terminally fused Bfr to H5gd based on the structure of bacterioferritin (PDB ID: 3E1J), respectively, were generated *in silico* in combination with the linker. The structures obtained by homology modeling were visualized using Pymol (Version 2.2.3, Schrödinger LLC, USA).

Construction of plasmids for protein expression

H5N1 (A/Indonesia/5/2005) hemagglutinin gene (GenBank ID: CY116646.1), H5N2 (A/aquatic bird/Korea/w81/2005) hemagglutinin gene (GenBank ID: GU361196.1), and vestigial esterase domain gene of H5N2 were synthesized by chemical synthesis (Bionics Co., Ltd., Korea). H5N1 HA globular domain (224 aa; 46–269 of H5N1 HA), H5N2 HA globular domain (224 aa; 62-285 of H5N2 HA), H5N2 HA vestigial esterase domain (triplet of 47 aa; 62-108 of H5N2 HA), and Bfr (158 aa of bacterioferritin) genes were obtained by PCR amplification. Amplified genes were inserted into pGE-mRID-3 and pGE-hRID-3 to yield plasmids pGE-RID-H5gd and pGE-RID-H5gd-Bfr, respectively. To construct RID-H5gd-Bfr and RID-Bfr, the Bfr gene was cloned into pGE-RID-H5gd and pGE-hRID-3. To obtain the RID(9m)-H5gd-Bfr, H5gd and Bfr genes were re-cloned into the pGE-hRBD(9m) plasmid. The H5N2 HAgd or VE domain genes were amplified by PCR and cloned into pGE-hRID-3, yielding pGE-RID-H5N2 HA gd or pGE-RID-H5N2 HA VE, respectively.

Protein expression and purification in E. coli

All plasmids, including RID-H5gd-Bfr, RID-Bfr, RID-H5gd, and RID(9m)-H5gd-Bfr, were transformed into the *E. coli* strain BL21(DE3)pLysS. The transformed cells were incubated at 37 °C until the optical density (OD_{600}) reached 0.5-0.6 at 600 nm. Proteins were expressed for 16 h at 18 °C by adding IPTG (0.5 mM). Cells (10 mL) were centrifuged at 3000 rpm for 10 min at 4 °C, suspended in PBS (0.3 mL), and lysed by sonication. Proteins in cell lysates were analyzed by SDS-PAGE as described previously.[33,34] Expressed proteins were purified by single-step nickel-affinity chromatography. The purified proteins (final glycerol concentration 20%) were stored at −80 °C until further use.

Size exclusion chromatography (SEC) for oligomeric status

The oligomeric status of purified recombinant proteins was analyzed by gel-filtration chromatography at 4 °C on a Superdex-200 analytical gel-filtration column (GE Healthcare). The column was equilibrated with buffer (50 mM Tris–HCl [pH 7.5], 100 mM NaCl, 2 mM 2-mercaptoethanol, 0.05% TritonX-100) and calibrated using broad range molecular weight markers, including ferritin (440 kDa), aldolase (158 kDa), and conalbumin (75 kDa) (GE Healthcare). After calibration, the sample proteins were injected and passed through a column with a buffer. Proteins separated by size were collected in tubes. Each protein

sample was mixed with 2× SDS loading buffer and analyzed by SDS-PAGE as described previously.[35]

RNA identification from RNA-protein complex

The cells were harvested, sonicated with lysis buffer, and separated into soluble and pellet fractions by centrifugation at 12,000 rpm for 15 min. Target proteins in the soluble fraction were purified using HisPur™ Ni-NTA Resin (Thermo Fisher Scientific) following the manufacturer's instructions. A 200 μL aliquot of each soluble fraction was further treated with 250 μg/mL of RNase A (iNtRON Biotechnology) and incubated at 37 °C for 15 min. Co-purification of the nucleic acids and proteins in the soluble fraction was performed on a native agarose gel. Nucleic acids were visualized with ethidium bromide staining, and the proteins were visualized using Coomassie blue staining.

Size measurement for self-assembled cNP

To measure the size of the particles of RID-H5gd-Bfr and RID(9m)-H5gd-Bfr, dynamic light scattering (DLS) was performed. Each sample (3 mL) was placed into a Dispo-H cell and analyzed using a zeta potential and particle size analyzer (ELS-2000ZS; Otsuka Electronics). The intensity distribution diameter of the nanoparticles was measured twice at 25 °C using water as a solvent with a sample accumulation time of 200 s.

Morphological analysis of cNP structure

Transmission electron microscopy (TEM) analysis was performed to visualize the cNP of RID-H5gd-Bfr and RID (9m)-H5gd-Bfr proteins. A drop of the proteins was placed onto a formvar/pure carbon-coated TEM grid (SPL). The grid was negatively stained with 2% uranyl acetate, dried, and examined using a JEM-F200 electron microscope (JEOL) at an accelerating voltage of 80 kV. The particle sizes were calculated using Camera-Megaview III (Soft Imaging, Systems, Germany) to measure the nanoparticles in random image fields.

Fetuin binding assay for HA on cNP

To investigate whether the purified recombinant proteins were folded properly, a fetuin-binding assay was performed. In brief, 200 μL of fetuin protein (Sigma-Aldrich) was coated on a 96-well immunoplate (Thermo Fisher, Waltham, MA, USA) at a concentration of 200 μg/mL and incubated overnight at 4 °C. Recombinant HAgd proteins (100 μL) were added to each well at various concentrations. The plates were analyzed as described in a previous study.[35]

Immunization and lethal challenge

Six-week-old female BALB/c mice (Orient Bio) were immunized with PBS (control) or RID-H5gd-Bfr, RID-Bfr, or RID-H5gd proteins (5 mice/group) adjuvanted with alum (Thermo Fisher, Waltham, MA, USA) via intraperitoneal injection (20 μg/100 μL/mouse). Each immunized mouse was administered a booster dose twice every 2 weeks (total 3 injections per mouse). Blood samples were collected via retro-orbital bleeding and centrifuged at 12,000 ×*g* for 30 min, and the immune sera were harvested from the supernatants. All serum samples were aliquoted and stored at −80 °C until further use. Three weeks after administering secondary boosting, all mice were challenged under anesthesia via intranasal administration of 5 MLD_{50}, 5×10^6 PFU of A/Indonesia/5/2005 (H5N1) reassortant virus, or 2 MLD_{50} of A/aquatic bird/Korea/w81/2005 (H5N2) virus with a mixture of PBS, alfaxalone, and xylazine (volume ratio 2:2:1; 100 μL/mouse).[36] The survival rate and weight change of the challenged mice were measured every day for 8 days.

Antibody binding assay of immunized serum

Enzyme-linked immunosorbent assay (ELISA) was performed to determine the titer of polyclonal antibodies in immunized mice. A 96-well immunoplate (Thermo Fisher, Waltham, MA, USA) was coated with 1×10^5 pfu rH5N1 live virus and maintained overnight at 4 °C (100 μL/well). The plates were analyzed as described in a previous study.[35]

Hemagglutination inhibition assay

A hemagglutination inhibition (HI) assay was performed to identify whether the serum antibody binds to the HA of the virus. Samples were treated with a receptor-destroying enzyme (RDE) to remove non-specific agglutination inhibitors and heated at 56 °C for 1 h. The sera were diluted with PBS in serial two-fold dilutions in 96-well plates. Equal volumes (50 μL) of influenza virus (4 hemagglutination units) were then added to the diluted sera, mixed, and incubated at 37 °C for 1 h. After incubation, an equal volume of 1% chicken erythrocytes was added and incubated at 4 °C for 1 h. The HI antibody titer of each serum sample was expressed as the reciprocal of the highest dilution of the sample that completely inhibited hemagglutination. The dilution of each serum with RDE and virus revealed that the detection limit of the HI assay was 8.

Antibody neutralization assay

Plaque reduction neutralization test (PRNT) was performed to measure neutralizing antibodies against H5N1 virus, as described in a previous study.[35] In brief, equal volumes of the H5N1 virus (100 PFU) were added to the diluted sera (1/25 dilution with PBS) and mixed. These mixtures were then adsorbed onto 24-well plates containing confluent Madin–Darby canine kidney (MDCK) cells. The agar overlaid plates were incubated at 32 °C in a 5% CO_2 incubator. The cell monolayers were stained with crystal violet for 4 days post-infection. Neutralization titers were calculated from dilutions that corresponded to a 50% plaque reduction compared to that observed with the control.

Identification of antibody binding to vestigial esterase domain

Western blot analysis was performed to identify antibody binding to the vestigial esterase (VE) domain using the final sera produced from immunized mice. Various dilutions of each serum sample were used to analyze the antibodies in the sera. Goat anti-mouse IgG antibody conjugated with HRP (Sigma-Aldrich, USA) was used as a secondary antibody. For the detection of antibodies against the VE domain in HA, 1 μg of H5N2 HAgd proteins or H5N2 HA VE domain proteins were loaded onto SDS-PAGE,

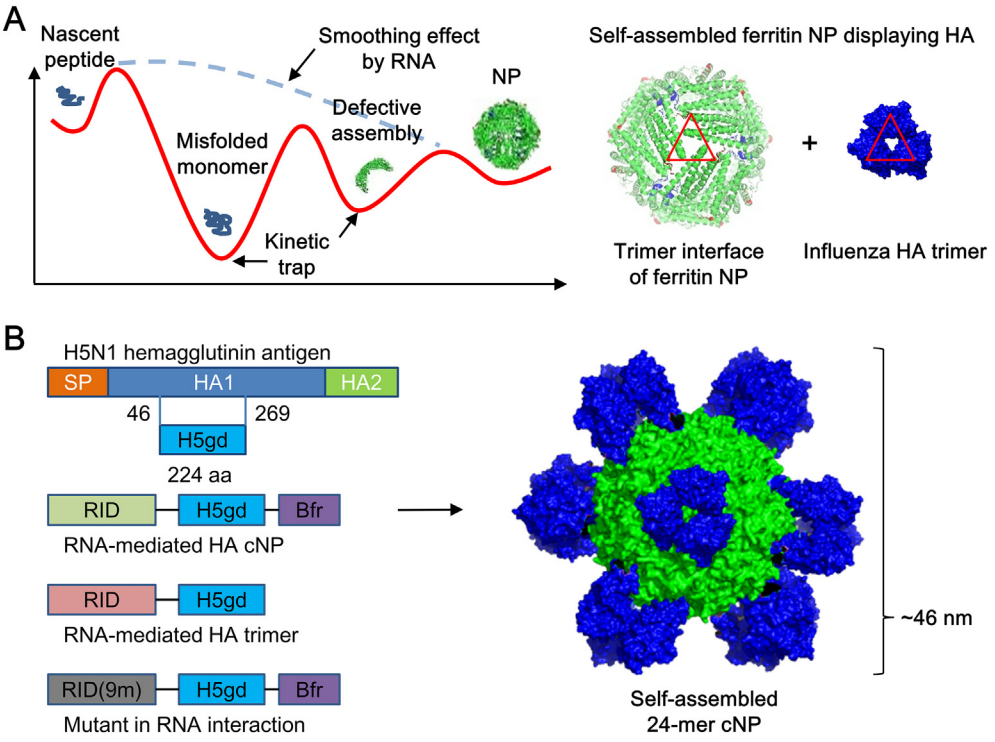

Figure 1. Nanoparticle formation of Bfr-fused proteins. **(A)** Schematic folding diagram with RNA-dependent chaperone for the assembly of ferritin NP and presentation of trimer interface of ferritin NP and H5gd. **(B)** Schematic constructs of H5gd antigen and schematic model of RID-H5gd-Bfr 24-mer nanoparticle. RID: RNA interaction domain; H5gd: target antigen; Bfr: NP scaffold; RID(9m): mutant of RID.

which were then subjected to western blotting with mouse serum (diluted by 1:1000), as described in a previous study.[35]

Ethics statement

All animal studies were performed according to the guidelines of the Ministry of Food and Drug Safety of the Republic of Korea. The protocol of the experiment was evaluated and approved by the IACUC of the International Vaccine Institute (Permit number: IACUC PN 2017-016). Five-week-old female BALB/c mice were purchased from Orient Bio Inc. (Seoul, Korea).

Statistical analysis

All data were analyzed with the unpaired *t* test for comparison between two columns in a two-tailed format using the GraphPad PRISM program (GraphPad, San Diego, CA, USA).

Results

Plasmid constructs for H5gd and nanoparticle design

The chaperoning role of RNAs in the folding of monomers and their subsequent assembly into cNPs is shown in Figure 1, *A*. A tri-partite monomeric antigen was designed (Figure 1, *B*). The RID represents the N-terminal appended domain (77 aa long) of human lysyl tRNA synthetase (KRS), which changes from a disordered structure into alpha-helical transition upon tRNA binding.[37] The construct is designed to display H5gd using the trimer axis at the N-terminal end of Bfr into an oligomeric nanoparticle structure, which might enhance the neutralizing capacity of antibodies.[18] First, we performed *in silico* structure modeling to investigate whether the fusion proteins could form 24-mer nanoparticles with outward protrusions of H5gd. To determine the domain of H5gd as an antigen, H1N1 (A/Puerto Rico/8/34) HA was compared with the H5N1 (A/Indonesia/5/2005) HA protein by 3D modeling. Considering the structural homology, the amino acid sequence from 46 to 269 of H5N1 HA (224 aa in length) was selected as the HAgd protein (data not shown). The H5gd protein was cloned into various protein expression vectors (Figure 1, *B* and Supplementary Figure 1). In parallel, RID(9m), a mutant form of RID where RNA does not bind, was used to monitor the effect of RNA binding on the solubility, folding, and assembly of the target proteins.[37] The schematic modeling of the nanoparticle assembly of the H5gd-Bfr protein is shown in Figure 1, *B*, right.

Oligomeric state of Bfr fusion proteins

Four different versions of proteins, H5gd, RID-H5gd, RID-H5gd-Bfr, and RID(9m)-H5gd-Bfr, were compared in terms of solubility (Supplementary Figure 2) and the ability to assemble NPs. To investigate the RNA binding ability of RID-H5gd-Bfr and RID(9m)-H5gd-Bfr, RNA-protein complexes were extracted after *E. coli* lysis. RNA was detected from RID-H5gd-Bfr but not from RID(9m)-H5gd-Bfr (Figure 2, *A*). As expected, the band disappeared after the RNase treatment. These results showed that the mutant could not bind to the RNA. Interestingly,

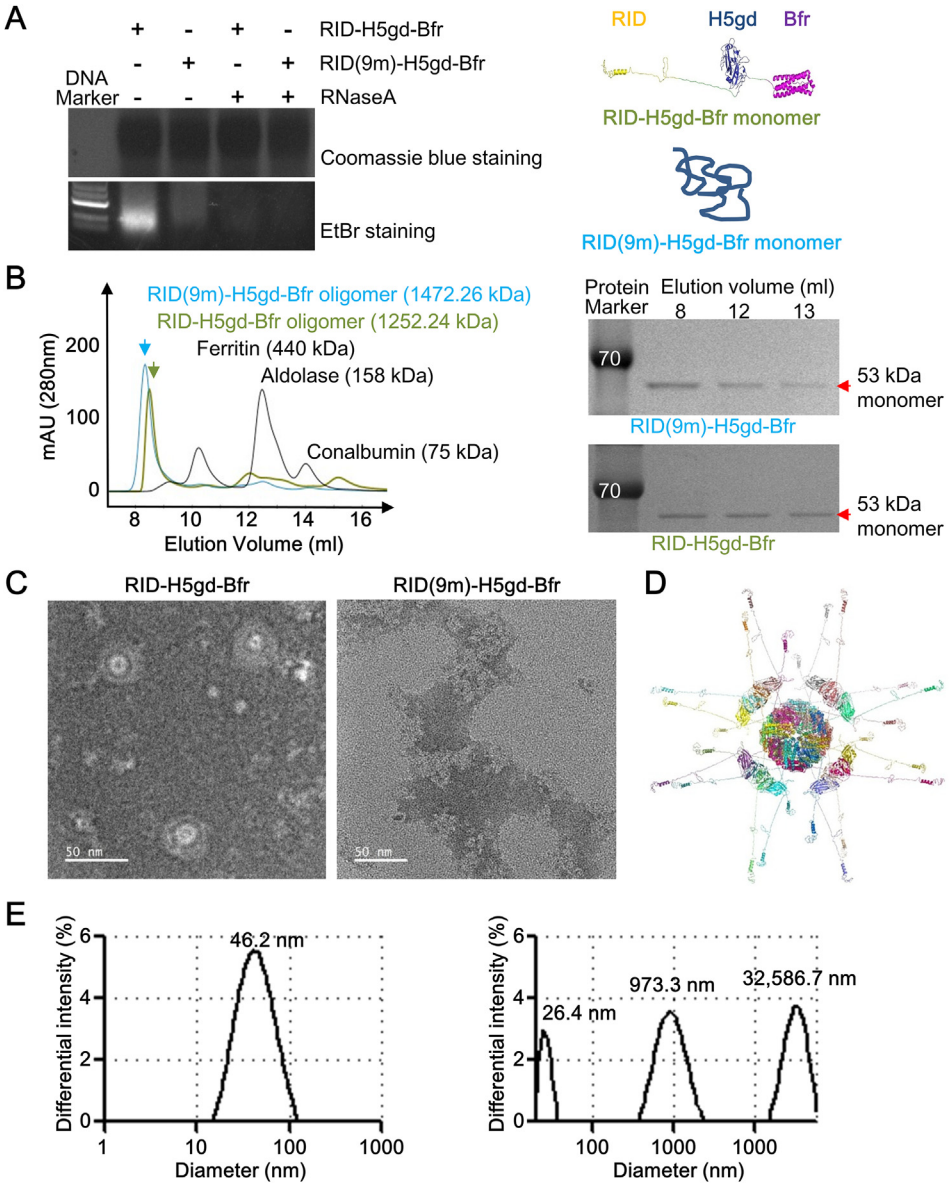

Figure 2. The role of RID in nanoparticle formation. **(A)** Detection of co-purified RNA from proteins with agarose gel (1%) analysis. **(B)** SEC of RID-H5gd-Bfr and RID(9m)-H5gd-Bfr with the calibration set (left). SDS-PAGE analysis of the eluted fractions derived from SEC (right). **(C)** TEM images of negatively stained RID-H5gd-Bfr (left) and RID(9m)-H5gd-Bfr (right). **(D)** 3D model of RID-H5gd-Bfr 24-mer cNP reconstructed by Pymol. **(E)** DLS analysis of RID-H5gd-Bfr (left) and RID(9m)-H5gd-Bfr (right).

the solubility of the tripartite fusion RID-H5gd-Bfr was similar to that of the RNA-binding mutation (Supplementary Figure 2, *C* and *D*). However, the mutants were predominantly amorphous aggregates (Figure 2). To purify and examine the oligomeric state of the expressed proteins, size-exclusion chromatography (SEC) was performed. Based on SEC data, the molecular weight of RID-H5gd-Bfr was estimated to be 1252 kDa, comparable to the expected size of 1267.2 kDa (Figure 2, *B*, left). For RID(9m)-H5gd-Bfr, the size estimated by SEC was 1472 kDa, which is slightly higher than the expected size of 1262.4 kDa. SDS-PAGE analysis confirmed the presence of proteins in each elution fraction (Figure 2, *B*, right). These results suggest that both RID-H5gd-Bfr and RID(9m)-H5gd-Bfr proteins are predominantly present in the oligomeric form, regardless of their RNA binding ability.

Effect of RNA on nanoparticle formation

The physicochemical properties of the assembled cNPs were examined using TEM and DLS. The TEM image of RID-H5gd-Bfr demonstrated nanoparticle-like structures: the inner circle of the nanoparticle represented the Bfr core, and the outer circle represented the RID-H5gd protein (Figure 2, *C*, left), with an estimated size of 45-50 nm. Compared to the dense core representing a structured ferritin scaffold, the relatively diffusive structure of the outer circle could be ascribed to the intrinsic

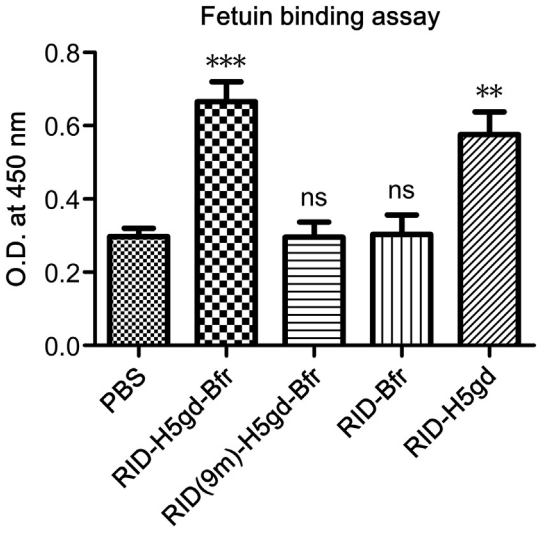

Figure 3. Assessment of trimeric HA formation by fetuin binding. ELISA was performed using fetuin glycoprotein as coating antigen. The comparisons of each column with PBS were analyzed by unpaired *t* test in two-tailed format. The data are expressed as mean ± SEM. $^{**}P < 0.01$; $^{***}P < 0.001$. ns: not significant.

disorder of the RID.[38] To investigate whether the increased size of cNP was caused by RID, structure modeling was performed with RID-H5gd-Bfr proteins, which were re-assembled into Bfr nanoparticles (PDB ID: 3E1J) using the Pymol program. The modeling of the nanoparticle assembly of the RID-H5gd-Bfr protein showed that the surface area of Bfr NP was sufficient to accommodate RID-H5gd without steric hindrance. Furthermore, it showed that the RID structure extended outward of the Bfr NP, increasing the size of the cNPs (Figure 2, *D*). However, the TEM image of RID(9m)-H5gd-Bfr showed aggregate-like structures (Figure 2, *C*, right). DLS analysis also confirmed that RID(9m)-H5gd-Bfr was present in an amorphous form without any structural regularity. RID-H5gd-Bfr protein was present in a homogeneous state with an estimated size of 46.2 nm (±19.7) in the solution (Figure 2, *E*, left). In contrast, RID(9m)-H5gd-Bfr was present as a heterogeneous mixture of variable sizes in the solution (Figure 2, *E*, right). Despite the SDS-PAGE showing the solubility of RID(9m)-H5gd-Bfr protein, the results showed that it was present predominantly as soluble amorphous aggregates. The results of SEC, TEM, and DLS together suggest that RNA interaction with RID is essential for the regular assembly of monomers into homogeneous cNPs.

Fetuin is a glycoprotein enriched with sialic acid, and the fetuin-HA interaction can be used to assess proper folding of HA in trimeric composition.[39,40] Strikingly, both RID-H5gd-Bfr and RID-H5gd proteins were bound to fetuin, whereas RID(9m)-H5gd-Bfr protein failed in the binding assay (Figure 3). The results indicate that RNA binding to RID is important not only for the proper folding of the H5gd monomer, but also for the assembly of monomers into nanoparticles. The physical stability of the cNPs was examined using DLS over 12 weeks of storage at 4 °C. The results showed that the nanostructure was stable for up to 11 weeks, with a gradual loss of integrity during prolonged storage (~10% at the 12th week) (Supplementary Figure 3).

Immunogenicity of H5gd vaccines

The efficacy of the self-assembled RID-H5gd-Bfr cNP was examined in a mouse model. Mice were vaccinated thrice, and each serum sample was collected to assess antibody responses (Supplementary Figure 4). In contrast, PBS or RID-Bfr, RID-H5gd-Bfr and RID-H5gd induced robust immunoglobulin (Ig) G antibodies against reassortant H5N1 virus (rH5N1) (Figure 4, *A*). ELISA data indicated that both RID-H5gd-Bfr and RID-H5gd proteins elicited IgG antibodies against the homologous virus, and the immunization boost further increased antibody titers (Supplementary Figure 5). The results showed that both recombinant proteins expressed in *E. coli* were highly immunogenic in mice.

Both RID-H5gd-Bfr and RID-H5gd elicited hemagglutination inhibition (HI) antibody titers (≥32) against rH5N1 virus after the second boost, whereas negative controls failed to elicit HI activity (Supplementary Figure 6). RID-H5gd elicited a higher level (~4 fold) of HI antibody titer against rH5N1 virus than RID-H5gd-Bfr (Figure 4, *B*). This may be partly attributed to the relatively smaller molar ratio of HAgd in the same amount of recombinant proteins (20 μg/mouse) used for immunization. Notably, RID-H5gd-Bfr elicited a remarkably higher level of neutralizing (NT) titer (~8 fold) against homologous rH5N1 virus (Figure 4, *C* and Supplementary Figure 7). This resulted in a 25-30 fold higher relative ratio of NT:HI titer for RID-H5gd-Bfr than that for RID-H5gd (Figure 4, *D*). It is noteworthy that the ferritin scaffold-mediated assembly of the H5gd antigen contributed significantly to improving the neutralizing capacity of the antibody.

Protection efficacy of H5gd vaccines

To investigate the protective efficacy of cNP vaccines, mice were challenged with rH5N1 viruses (5 MLD_{50}; 5×10^6 PFU) after vaccination. All mice that received RID-H5gd-Bfr or RID-H5gd survived the lethal challenge (Figure 5, *A*). The maximum weight loss of mice was 6% and 9% for RID-H5gd-Bfr and RID-H5gd, respectively, and all mice recovered after 8 days (Figure 5, *B*). In contrast, mice that were administered PBS or RID-Bfr demonstrated >20% loss in body weight, and all succumbed within 6 days. These results suggest that both RID-H5gd-Bfr and RID-H5gd successfully protected the mice from lethal challenge with homologous virus.

To evaluate the potential cross-protection against the heterologous virus, mice were challenged with mouse-adapted H5N2 virus (2 MLD_{50}) after vaccination (sequence homology of HA, ~88.4%).[41] Control mice that received PBS or RID-Bfr showed rapid weight loss and succumbed within 6 days after the lethal H5N2 challenge. However, mice vaccinated with RID-H5gd-Bfr, but not RID-H5gd, survived the H5N2 heterologous challenge with a weight loss of <4% (Figure 5, *C* and *D*). These results showed that the formation of cNPs provides cross-protection against heterologous lethal challenge. Overall, RID-H5gd-Bfr (cNP) demonstrated superior and broader protection against both homologous and heterologous challenges compared to RID-H5gd (trimer), making it a powerful tool for inducing cross-protective immune responses.

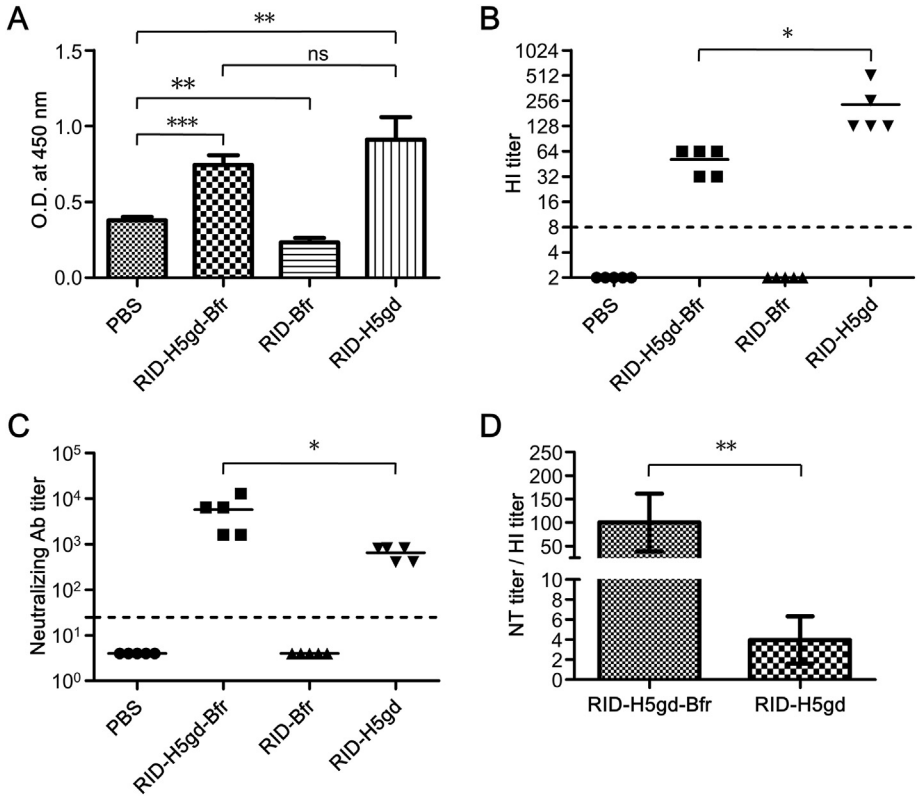

Figure 4. Immunogenicity of H5gd fusion proteins. Groups of mice were immunized with indicated proteins thrice. **(A)** Serum IgG antibody determined by ELISA. The data are expressed as mean ± SEM. **(B)** HI titer determined by the HI assay. **(C)** NT titer determined by PRNT. The dashed line indicates the detection limit of HI assay and PRNT, respectively. **(D)** The ratio of NT and HI titer of each serum. ns: not significant. The data are expressed as mean ± SD. All data were analyzed by unpaired *t* test in a two-tailed format. **P*< 0.05; ***P*< 0.01; ****P*< 0.001.

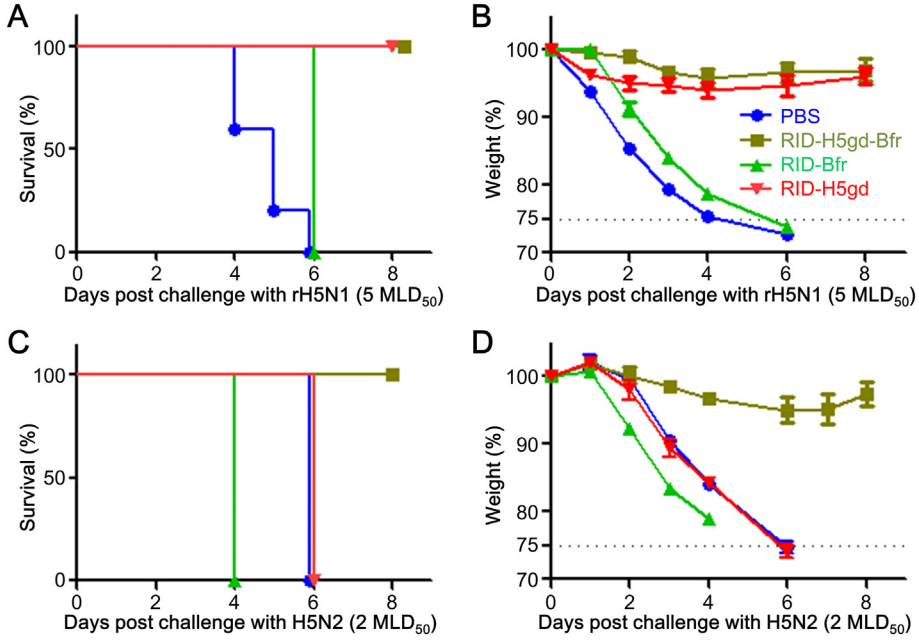

Figure 5. Protective efficacy against homologous or heterologous challenge in mice. Groups of mice were immunized with indicated proteins thrice. **(A)** Survival rate of mice after homologous rH5N1 challenge. **(B)** Body weights of mice after rH5N1 challenge. rH5N1 challenge data represent four groups with $n = 5$ mice/group. **(C)** Survival rate of mice after heterologous H5N2 challenge. **(D)** Body weights of mice after H5N2 challenge. H5N2 challenge data represent four groups with $n = 4$ mice/group. n = the number of mice used in the lethal challenge test.

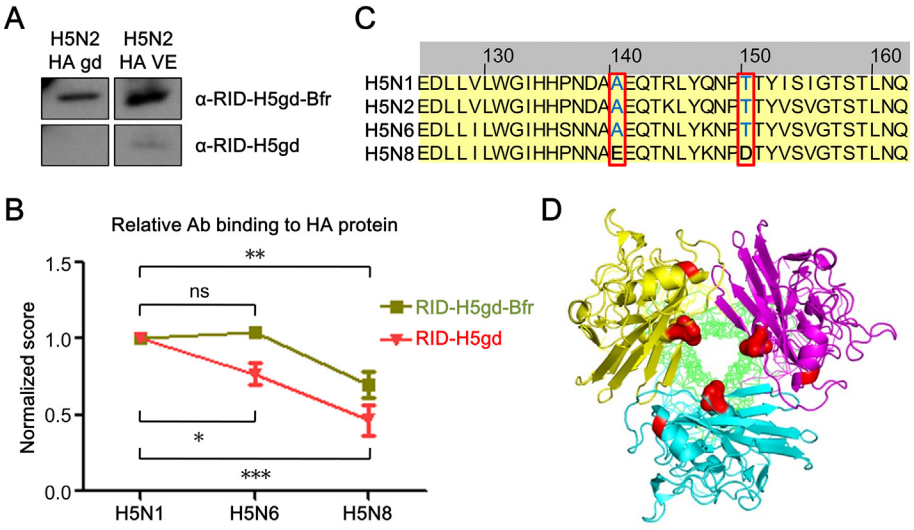

Figure 6. Cross-clade reactivity of the serum immunized with H5gd fusion proteins. **(A)** Western blot analysis of immunized serum for the identification of IgG bound to HA VE domain. **(B)** Comparison of the serum IgG bound to sub-clade HA proteins as observed with ELISA. The normalized scores of each column are analyzed by unpaired *t* test in a two-tailed format. The data are expressed as mean ± SEM. **P*< 0.05; ***P*< 0.01; ****P*< 0.001. ns: not significant. **(C)** Alignment of HA proteins of H5N1, H5N2, H5N6, H5N8. The red box indicates identical amino acids in H5N1, H5N2, H5N6 (not in H5N8). **(D)** 3D model of HA protein trimer. The red color represents modified amino acids on a trimer core of H5N8 HA.

Cross-clade reactivity of H5gd vaccines

To determine immunological correlates for the cross-protection of the nanoparticle vaccine, we measured the antibody-dependent cellular cytotoxicity (ADCC) activity of sera antibodies, which is associated with a cross-reactive immune response.[42] However, the ADCC activity against H5N2 virus-infected MDCK cells was below the detection level (data not shown). We then investigated antibodies directed toward the vestigial esterase (VE) domain, which is conserved in the HA globular domain among influenza viruses and is known to provide cross-protection.[43,44] Notably, western blot analysis showed a VE domain-specific immune response in the RID-H5gd-Bfr sera, but not in the RID-H5gd immune sera (Figure 6, *A*). This result suggests that the assembly of NPs triggers the induction of antibodies against the conserved VE domain.

To investigate the differences in the top of the trimeric region in HA proteins, ELISA was performed using serum antibodies against the HA proteins of H5N1, H5N6, and H5N8. As shown in Figure 6, *B*, H5gd exhibited cross-clade reactivity with H5N6 and the recently discovered H5N8. Interestingly, serum elicited by RID-H5gd-Bfr cNP exhibited more potent binding to sub-clade HA proteins of H5N6 and H5N8 than H5gd without NP formation. The sequence homology of HA was compared among various H5 subtypes (Figure 6, *C*), and variations within the conserved receptor-binding region are displayed on the 3D model of HA (Figure 6, *D*). Taken together, the nanoparticle-based H5gd vaccine can provide cross-clade reactivity, conferring broader protection against heterologous viruses.

Discussion

Nanoparticle vaccines have distinctive features of size and geometry, which are critical for their potent ability to activate B cells, thereby eliciting robust antibody responses. Multivalent epitopes are displayed in a highly repetitive manner, leading to cross-linking of B cell receptors, which stimulate B cells to induce potent and long-lasting antibody responses.[4,45,46] Especially for developing cNP vaccines comprising multiple functional domains, serious considerations should be given to robust and faithful production platforms. Bacterial expression systems can be easily scaled up and are the least expensive among various platforms.[10] A major drawback for the bacterial host, however, is that it does not provide an optimal environment for the folding and assembly of antigens, and thus, is rarely successful for cNP assembly.

Here, we show the assembly of viral capsids guided by RNAs in the bacterial cytoplasm into genome-free, non-infectious empty nanoparticles. The novel function of RNAs as chaperones (chaperna)[33,35] was harnessed for the assembly of HPAIV HAgd monomers into immunologically potent, highly ordered repetitive structures, as confirmed by TEM and DLS (Figure 2). The soluble tripartite fusion protein was purified and self-assembled into the expected size of the nanostructure. Notably, RNA interaction was essential for the regular assembly of monomers, overcoming the kinetic barrier over defective assemblages (Figures 2 and 3). Immunization of mice with the nanoparticles induced robust HI and virus-neutralizing (NT) antibodies and protected the mice from lethal challenge, not only with the homologous H5N1, but also with heterologous H5N2. Although the influenza-induced lung pathology was not examined, the virulence reflected by weight loss and mortality confirmed effective protection from lethal challenges (Figure 5). Surprisingly, the ratio between the two independent correlates of protection (NT/HI) was significantly elevated (up to 30 fold) by the NP assembly of HA as a nanostructure (Figure 4). Although the HI titer has long been adopted as the major marker for the protective efficacy of the influenza vaccine, regulatory

authorities advise NT titer as an additional criterion for vaccine efficacy.[47,48] Compared to the HI titer, which measures the ability of the inhibition of cell-virus interaction, NT represents a direct measure for inactivation of the infecting virus. Thus, a potent increase in the NT titer in the present NP-based vaccine (Figure 4) may be implemented to improve the influenza vaccine.

Moreover, NP assembly triggered antibodies against a conserved VE domain in HA. Overall, the observed immune modulation was manifested in cross-protection from the heterologous H5N2 virus (Figure 5). It should be noted that the current approach for developing a 'universal' influenza vaccine (UIV) relies on immune reprogramming, redirecting the immune response from the variable region that provides strain-specific protection into a conserved region that would provide broad protection against genetic variant strains.[49,50] Recently, a study showed that the display of HA of multiple lineages in a single particle significantly increased cross-protection.[51] Although the mechanism of immune re-direction into the conserved VE domain via NP assembly remains to be elucidated (Figure 6), the present results address the design of broadly protective HPAIV vaccines. A recent report has characterized multiple immune correlates for broad protection, including antibody effector functions, T cell responses, and mucosal immunity,[49] although these effects were not evaluated in the present study.

Besides contributing to the global issue of the pandemic, outstanding questions remain regarding the mechanism of RNA-dependent assembly of nanoparticles. First, mimicking well-known protein-based molecular chaperones, RNA molecules can prevent misfolding of proteins via hydrophobic shielding of the folding intermediates[52], as observed in both natural systems[53] and engineered recombinant systems.[35,54] Preventing intermolecular aggregation facilitates intramolecular folding of proteins into their functional conformation. Notably, various types of hydrophobic interactions have been observed in RNA-protein (RNP) complexes,[55] which may also operate in *de novo* folding processes. Second, RNA binding exerts strong electrostatic repulsion among monomers, preventing intermolecular interactions among highly unstable/unstructured folding intermediates that lead to the chaotic consequences of misfolding and aggregation (Figure 1, *A*). This allows a soluble, monodisperse state of the 'molten globule' into an intramolecular structural rearrangement for folding into a stable structure.[56] This would keep the antigen in an 'assembly-ready' monomeric status; however, upon dissociation of RNA molecules, the monomers begin to assemble into multimers. It is conceivable that the intrinsic disorder of RID and the conformational changes induced by tRNA binding[38] may further contribute to the kinetic control of this process, preventing the accumulation of unstable intermediates haphazardly leading to misfolding/defective assembly (Figure 1, *A*). Likened to a 'social-distancing' measure for minimizing the catastrophic consequences of COVID-19,[57] RNA operates a chaperone function for the quality control of the NP structure into immunologically relevant conformations.[58]

In conclusion, a versatile nanoassembly platform tailored to cNP vaccines was established. A regular assembly of monomeric antigen into the nanostructure was enabled by harnessing the RNA-based chaperna function, overcoming the kinetic trap of misfolding/defective assembly. The results provide a design principle for the production of cross-protective vaccines against various influenza strains. The results not only address pandemic preparedness by introducing a strategy for the fast delivery of low-cost vaccines, but also the basic protein folding/assembly mechanism associated with the chaperone action.

Author contributions

Jongkwan Lim: Methodology, Investigation, Validation, Formal analysis, Visualization, Writing – original draft, Writing – review & editing; Yucheol Cheong: Investigation, Formal analysis; Young-Seok Kim: Investigation; Wonil Chae: Investigation; Beom Jeung Hwang: Investigation; Jinhee Lee: Investigation; Yo Han Jang: Methodology, Formal analysis, Visualization; Young Hoon Roh: Methodology, Formal analysis, Visualization, Writing – original draft, Writing – review & editing, Supervision; Sang-UK Seo: Formal analysis, Visualization, Writing – original draft, Writing – review & editing, Supervision; Baik L. Seong: Conceptualization, Methodology, Investigation, Validation, Formal analysis, Writing – original draft, Writing – review & editing, Supervision, Funding acquisition.

Acknowledgments

This work was supported by the Korea Health Technology R&D Project through the Korea Health Industry Development Institute (KHIDI), the Ministry of Health & Welfare, Republic of Korea [grant number HV20C0070]; the National Research Foundation of Korea [grant number 2018M3A9H4079358]; Brain Korea 21 (BK21) FOUR program.

Appendix A. Supplementary data

Supplementary data to this article can be found online at https://doi.org/10.1016/j.nano.2021.102438.

References

1. Mehand MS, Al-Shorbaji F, Millett P, Murgue B, The WHO. R&D blueprint: 2018 review of emerging infectious diseases requiring urgent research and development efforts. *Antiviral Res* 2018;**159**:63-7.
2. Andre FE, Booy R, Bock HL, Clemens J, Datta SK, John TJ, et al. Vaccination greatly reduces disease, disability, death and inequity worldwide. *Bull World Health Organ* 2008;**86**:140-6.
3. Wang N, Shang J, Jiang S, Du L. Subunit vaccines against emerging pathogenic human coronaviruses. *Front Microbiol* 2020;**11**:298.
4. Bachmann MF, Jennings GT. Vaccine delivery: a matter of size, geometry, kinetics and molecular patterns. *Nat Rev Immunol* 2010;**10**:787-96.
5. Mohsen MO, Zha L, Cabral-Miranda G, Bachmann MF. Major findings and recent advances in virus-like particle (VLP)-based vaccines. *Semin Immunol* 2017;**34**:123-32.
6. Kushnir N, Streatfield SJ, Yusibov V. Virus-like particles as a highly efficient vaccine platform: diversity of targets and production systems and advances in clinical development. *Vaccine* 2012;**31**:58-83.
7. Zhang X, Wei M, Pan H, Lin Z, Wang K, Weng Z, et al. Robust manufacturing and comprehensive characterization of recombinant hepatitis E virus-like particles in Hecolin((R)). *Vaccine* 2014;**32**:4039-50.

8. Le DT, Radukic MT, Muller KM. Adeno-associated virus capsid protein expression in Escherichia coli and chemically defined capsid assembly. *Sci Rep* 2019;**9**:18631.
9. Ulmer JB, Valley U, Rappuoli R. Vaccine manufacturing: challenges and solutions. *Nat Biotechnol* 2006;**24**:1377-83.
10. Jeong H, Seong BL. Exploiting virus-like particles as innovative vaccines against emerging viral infections. *J Microbiol* 2017;**55**:220-30.
11. McLellan JS, Chen M, Joyce MG, Sastry M, Stewart-Jones GB, Yang Y, et al. Structure-based design of a fusion glycoprotein vaccine for respiratory syncytial virus. *Science* 2013;**342**:592-8.
12. Rivera M. Bacterioferritin: structure, dynamics, and protein-protein interactions at play in iron storage and mobilization. *Acc Chem Res* 2017;**50**:331-40.
13. Yariv J, Kalb AJ, Sperling R, Bauminger ER, Cohen SG, Ofer S. The composition and the structure of bacterioferritin of Escherichia coli. *Biochem J* 1981;**197**:171-5.
14. Galloway AL, Murphy A, DeSimone JM, Di J, Herrmann JP, Hunter ME, et al. Development of a nanoparticle-based influenza vaccine using the PRINT technology. *Nanomedicine* 2013;**9**:523-31.
15. Babapoor S, Neef T, Mittelholzer C, Girshick T, Garmendia A, Shang H, et al. A novel vaccine using nanoparticle platform to present immunogenic M2e against avian influenza infection. *Influenza Res Treat* 2011;**2011**:126794.
16. Bolduc M, Baz M, Laliberte-Gagne ME, Carignan D, Garneau C, Russel A, et al. The quest for a nanoparticle-based vaccine inducing broad protection to influenza viruses. *Nanomedicine* 2018;**14**:2563-74.
17. Yassine HM, Boyington JC, McTamney PM, Wei CJ, Kanekiyo M, Kong WP, et al. Hemagglutinin-stem nanoparticles generate heterosubtypic influenza protection. *Nat Med* 2015;**21**:1065-70.
18. Kanekiyo M, Wei CJ, Yassine HM, McTamney PM, Boyington JC, Whittle JR, et al. Self-assembling influenza nanoparticle vaccines elicit broadly neutralizing H1N1 antibodies. *Nature* 2013;**499**:102-6.
19. Raghunandan R, Lu H, Zhou B, Xabier MG, Massare MJ, Flyer DC, et al. An insect cell derived respiratory syncytial virus (RSV) F nanoparticle vaccine induces antigenic site II antibodies and protects against RSV challenge in cotton rats by active and passive immunization. *Vaccine* 2014;**32**:6485-92.
20. Glenn GM, Smith G, Fries L, Raghunandan R, Lu H, Zhou B, et al. Safety and immunogenicity of a Sf9 insect cell-derived respiratory syncytial virus fusion protein nanoparticle vaccine. *Vaccine* 2013;**31**:524-32.
21. Lai S, Qin Y, Cowling BJ, Ren X, Wardrop NA, Gilbert M, et al. Global epidemiology of avian influenza A H5N1 virus infection in humans, 1997-2015: a systematic review of individual case data. *Lancet Infect Dis* 2016;**16**: e108 e18.
22. Manini I, Trombetta CM, Lazzeri G, Pozzi T, Rossi S, Montomoli E. Egg-independent influenza vaccines and vaccine candidates. *Vaccines (Basel)* 2017;**5**:1-8.
23. Yamada S, Yasuhara A, Kawaoka Y. Soluble recombinant hemagglutinin protein of H1N1pdm09 influenza virus elicits cross-protection against a lethal H5N1 challenge in mice. *Front Microbiol* 2019;**10**:2031.
24. Wang K, Holtz KM, Anderson K, Chubet R, Mahmoud W, Cox MM. Expression and purification of an influenza hemagglutinin—one step closer to a recombinant protein-based influenza vaccine. *Vaccine* 2006;**24**:2176-85.
25. Margine I, Krammer F, Hai R, Heaton NS, Tan GS, Andrews SA, et al. Hemagglutinin stalk-based universal vaccine constructs protect against group 2 influenza A viruses. *J Virol* 2013;**87**:10435-46.
26. Prabakaran M, He F, Meng T, Madhan S, Yunrui T, Jia Q, et al. Neutralizing epitopes of influenza virus hemagglutinin: target for the development of a universal vaccine against H5N1 lineages. *J Virol* 2010;**84**:11822-30.
27. Chen TH, Liu WC, Lin CY, Liu CC, Jan JT, Spearman M, et al. Glycan-masking hemagglutinin antigens from stable CHO cell clones for H5N1 avian influenza vaccine development. *Biotechnol Bioeng* 2019;**116**:598-609.
28. Khurana S, Verma S, Verma N, Crevar CJ, Carter DM, Manischewitz J, et al. Bacterial HA1 vaccine against pandemic H5N1 influenza virus: evidence of oligomerization, hemagglutination, and cross-protective immunity in ferrets. *J Virol* 2011;**85**:1246-56.
29. Arakawa T. Expression and refolding technologies for production of recombinant proteins. *Curr Pharm Biotechnol* 2010;**11**:231-2.
30. Vermasvuori R, Koskinen J, Salonen K, Siren N, Weegar J, Dahlbacka J, et al. Production of recombinant HIV-1 nef protein using different expression host systems: a techno-economical comparison. *Biotechnol Prog* 2009;**25**:95-102.
31. Yamaguchi H, Miyazaki M. Refolding techniques for recovering biologically active recombinant proteins from inclusion bodies. *Biomolecules* 2014;**4**:235-51.
32. Son A, Horowitz S, Seong BL. Chaperna: linking the ancient RNA and protein worlds. *Rna Biol* 2021;**18**:16-23.
33. Son A, Choi SI, Han G, Seong BL. M1 RNA is important for the in-cell solubility of its cognate C5 protein: Implications for RNA-mediated protein folding. *Rna Biol* 2015;**12**:1198-208.
34. Kwon SB, Kim P, Woo HS, Kim TY, Kim JY, Lee HM, et al. Recombinant adenylate kinase 3 from liver fluke Clonorchis sinensis for histochemical analysis and serodiagnosis of clonorchiasis. *Parasitology* 2018;**145**:1531-9.
35. Yang SW, Jang YH, Kwon SB, Lee YJ, Chae W, Byun YH, et al. Harnessing an RNA-mediated chaperone for the assembly of influenza hemagglutinin in an immunologically relevant conformation. *FASEB J* 2018;**32**:2658-75.
36. Jang YH, Jung EJ, Byun YH, Lee KH, Lee EY, Lee YJ, et al. Immunogenicity and protective efficacy of cold-adapted X-31 live attenuated pre-pandemic H5N1 influenza vaccines. *Vaccine* 2013;**31**:3339-46.
37. Kwon SB, Yu JE, Park C, Lee J, Seong BL. Nucleic acid-dependent structural transition of the intrinsically disordered n-terminal appended domain of human Lysyl-tRNA synthetase. *Int J Mol Sci* 2018;**19**:1-16.
38. Agou F, Yang Y, Gesquiere JC, Waller JP, Guittet E. Polyanion-induced alpha-helical structure of a synthetic 23-residue peptide representing the lysine-rich segment of the N-terminal extension of yeast cytoplasmic aspartyl-tRNA synthetase. *Biochemistry* 1995;**34**:569-76.
39. de Vries RP, de Vries E, Bosch BJ, de Groot RJ, Rottier PJ, de Haan CA. The influenza A virus hemagglutinin glycosylation state affects receptor-binding specificity. *Virology* 2010;**403**:17-25.
40. de Vries RP, de Vries E, Martinez-Romero C, McBride R, van Kuppeveld FJ, Rottier PJ, et al. Evolution of the hemagglutinin protein of the new pandemic H1N1 influenza virus: maintaining optimal receptor binding by compensatory substitutions. *J Virol* 2013;**87**:13868-77.
41. Song MS, Pascua PN, Lee JH, Baek YH, Lee OJ, Kim CJ, et al. The polymerase acidic protein gene of influenza a virus contributes to pathogenicity in a mouse model. *J Virol* 2009;**83**:12325-35.
42. Zhong W, Gross FL, Holiday C, Jefferson SN, Bai Y, Liu F, et al. Vaccination with 2014-15 seasonal inactivated influenza vaccine elicits cross-reactive anti-HA antibodies with strong ADCC against antigenically drifted circulating H3N2 virus in humans. *Viral Immunol* 2016;**29**:259-62.
43. Paul SS, Mok CK, Mak TM, Ng OW, Aboagye JO, Wohlbold TJ, et al. A cross-clade H5N1 influenza A virus neutralizing monoclonal antibody binds to a novel epitope within the vestigial esterase domain of hemagglutinin. *Antiviral Res* 2017;**144**:299-310.
44. Zheng Z, Paul SS, Mo X, Yuan YA, Tan YJ. The vestigial esterase domain of haemagglutinin of H5N1 avian influenza A virus: antigenicity and contribution to viral pathogenesis. *Vaccines (Basel)* 2018;**6**:1-12.
45. Zabel F, Kundig TM, Bachmann MF. Virus-induced humoral immunity: on how B cell responses are initiated. *Curr Opin Virol* 2013;**3**:357-62.
46. Jennings GT, Bachmann MF. The coming of age of virus-like particle vaccines. *Biol Chem* 2008;**389**:521-36.
47. Heeringa M, Leav B, Smolenov I, Palladino G, Isakov L, Matassa V. Comparability of titers of antibodies against seasonal influenza virus strains as determined by hemagglutination inhibition and microneutralization assays. *J Clin Microbiol* 2020;**58**:1-10.
48. Lin Y, Gu Y, Wharton SA, Whittaker L, Gregory V, Li X, et al. Optimisation of a micro-neutralisation assay and its application in antigenic characterisation of influenza viruses. *Influenza Other Respir Viruses* 2015;**9**:331-40.
49. Jang YH, Seong BL. Call for a paradigm shift in the design of universal influenza vaccines by harnessing multiple correlates of protection. *Expert Opin Drug Discov* 2020;**15**:1441-55.

50. Jang YH, Seong BL. The quest for a truly universal influenza vaccine. *Front Cell Infect Microbiol* 2019;**9**:344.
51. Kanekiyo M, Joyce MG, Gillespie RA, Gallagher JR, Andrews SF, Yassine HM, et al. Mosaic nanoparticle display of diverse influenza virus hemagglutinins elicits broad B cell responses. *Nat Immunol* 2019;**20**:362-72.
52. Choi SI, Ryu K, Seong BL. RNA-mediated chaperone type for de novo protein folding. *RNA Biol* 2009;**6**:21-4.
53. Kim JM, Choi HS, Seong BL. The folding competence of HIV-1 Tat mediated by interaction with TAR RNA. *Rna Biol* 2017;**14**:926-37.
54. Lee J, Son A, Kim P, Kwon SB, Yu JE, Han G, et al. RNA-dependent chaperone (chaperna) as an engineered pro-region for the folding of recombinant microbial transglutaminase. *Biotechnol Bioeng* 2019;**116**:490-502.
55. Draper DE. Themes in RNA-protein recognition. *J Mol Biol* 1999;**293**:255-70.
56. Lindhoud S, Pirchi M, Westphal AH, Haran G, van Mierlo CP. Gradual folding of an off-pathway molten globule detected at the single-molecule level. *J Mol Biol* 2015;**427**:3148-57.
57. Lewnard JA, Lo NC. Scientific and ethical basis for social-distancing interventions against COVID-19. *Lancet Infect Dis* 2020;**20**:631-3.
58. Choi SI, Seong BL. A social distancing measure governing the whole proteome. *Curr Opin Struct Biol* 2020;**66**:104-11.